KURENAI
Kyoto University Research Information Repository

KYOTO UNIVERSITY

Title	Fabrication of carbon nanotube/NiOx(OH)y nanocomposite by pulsed electrodeposition for supercapacitor applications
Author(s)	Hakamada, Masataka; Moriguchi, Akitoshi; Mabuchi, Mamoru
Citation	Journal of Power Sources (2014), 245: 324-330
Issue Date	2014-01
URL	http://hdl.handle.net/2433/176997
Right	© 2013 Elsevier B.V.
Type	Journal Article
Textversion	author

Kyoto University

Fabrication of carbon nanotube/$NiO_x(OH)_y$ nanocomposite by pulsed electrodeposition for supercapacitor applications

Masataka HAKAMADA*, Akitoshi MORIGUCHI, Mamoru MABUCHI

Department of Energy Science and Technology, Graduate School of Energy Science,

Kyoto University, Yoshidahonmachi, Sakyo, Kyoto 606-8501, Japan

* Corresponding author. Tel: +81-75-753-5427; fax: +81-75-753-5428. E-mail: hakamada.masataka.3x@kyoto-u.ac.jp (M. Hakamada).

Abstract

Nanocomposite films based on carbon nanotubes (CNTs)/ nickel (Ni)-species were fabricated by electrophoretic deposition (EPD) of CNT, followed by pulsed electrodeposition of Ni and annealing in air. $NiO/Ni(OH)_2$ particles with 7 ± 4 nm diameters were uniformly dispersed on the CNT networks. Cyclic voltammetry revealed that the CNT/$NiO_x(OH)_y$ nanocomposite films had high specific capacitances of 1451, 1158, 998, 896 and 851 F/g per mass of active Ni species at 1, 10, 30, 50 and 100 mV/s, respectively, in the potential window of 0.4 V. An annealing time of 1 h (at 523 K) enhanced the pseudocapacity of deposited Ni species by the dehydration of $Ni(OH)_2$ to form NiO. Longer annealing time reduced the capacitance because of sintering and subsequent decrease in surface area of Ni deposits. The capacitance of the fabricated CNT/$NiO_x(OH)_y$ nanocomposite was maintained after 20000 cycles of potential sweeping.

Keywords: carbon nanotube; nickel oxide; nanocomposite; pulsed electrodeposition; pseudocapacitance

1. Introduction

First reported by Iijima [1], carbon nanotubes (CNTs) have drawn considerable attention in material sciences. Multi-walled CNTs form three-dimensional networks and are frequently used as thin films in applications such as capacitors, actuators and displays [2]. Electrophoretic deposition (EPD) can be used to fabricate CNT into films with micrometer-scale thickness [3]. Thin films of CNTs are good candidates for high surface area support materials. In addition, the high electrical conductivity of multi-walled CNTs distinguishes them from other porous supports such as mesoporous silica and titania.

Nanocomposites of CNT and Ni species are promising for applications in capacitors [4], hydrogen storage [5,6] and hydrogenation catalysis [7]. In particular, CNT/NiO or CNT/Ni(OH)$_2$ nanocomposites show potential for applications in capacitors [8–19]. Capacitors are energy storage devices that may be become a backup power source for hybrid vehicles. Compared with batteries, capacitors generally feature lower energy densities but greater cycling capacity [20]. Energy density is represented by $1/2CV^2$, where C is capacitance and V is voltage between the two electrodes [20]. Current challenges in capacitor development are the simultaneous achievement of high capacitance and voltage windows. Recently, metal oxides such as NiO [8–19], RuO$_2$ [21,22] and MnO$_2$ [23] have received attention as promising materials for a type of pseudocapacitors. These pseudocapacitors use a redox reaction at the surface of the oxides for energy storage. The theoretical capacitances of NiO and Ni(OH)$_2$ are 2584 F/g and 2082 F/g within 0.5 V [14,24].

CNT/Ni-species (including Ni, NiO, Ni(OH)$_2$) nanocomposites may be effectively fabricated by electroless plating [4–7], electroplating [8,10–12,15,25,26], impregnation

2

[27,28] and other processes [9,16,18]. Pulsed electrodeposition, in which the applied potential is oscillated at high frequencies during deposition of metals, is another strategy to fabricate nanostructured Ni [29,30]. In this study, we carried out pulsed electrodeposition of Ni on CNTs and annealing in air to make a CNT/NiO$_x$(OH)$_y$ nanocomposite. We investigated capacitive properties of the CNT/NiO$_x$(OH)$_y$ by cyclic voltammetry (CV) and chronopotentiometry (CP).

2. Experimental

Commercially available multi-walled CNTs (FloTube 9000, prepared by a catalytic vapor deposition process) were purchased from CNano Technology Ltd (Santa Clara, US). The raw CNTs were first treated in a concentrated mixture of 15.6 mol/L nitric acid and 18 mol/L sulfuric acid (with volumetric ratio of 1 : 3) at 333 K for 8 h. The treated CNTs were then washed several times by ultrasonication in distilled water to remove excess acid.

Following the acid treatment, EPD was carried out to fabricate the CNT film. The negative and positive electrodes were Pt and SUS316L (The Nilaco Corp., Tokyo, Japan) foils with exposed areas of 20×25 mm^2 and thickness of 20 μm, respectively. The distance between the electrodes was 20 mm. The acid-treated CNTs were suspended at a concentration of 1 g/L in distilled water for EPD. A voltage of 30 V was applied between the electrodes at room temperature (298 K) for 90 s. After the EPD, the CNTs film was dried in air and then heated at 673 K for 3 h to oxidize and insulate the SUS316L substrate. This oxidation step facilitated preferential electrodeposition of Ni on CNTs rather than the SUS316L substrate. Pulsed electrodeposition of Ni was carried out on the CNTs film to form CNTs/Ni nanocomposite film. The pulsed current is

shown in Fig. S1 (in Supplementary Data) with maximum current densities of 3 and 0.03 A/cm^2 applied for 0.5 and 50 s, respectively. These current densities were calculated from division of the current by the apparent exposed area (5 cm^2). The electrolyte was composed of $NiSO_4 \cdot 6H_2O$ (240 g/L), $NiCl_2 \cdot 6H_2O$ (45 g/L), H_3BO_3 (35 g/L) and $C_7H_5NO_3S$ (saccharin, 2.4 g/L). The CNTs substrate made up the cathode and Ni plate (The Nilaco Corp., Japan) was used for the anode. The temperature was maintained at 323 K during the pulsed electrodeposition. After electrodeposition, the CNTs/Ni nanocomposite film was washed with distilled water several times and dried in air. Several samples were annealed in air to oxidize Ni, at temperatures of 473, 523 or 573 K for durations of 1 and 72 h.

The samples were observed by a scanning electron microscope (SEM, SU-6600 by Hitachi High-Technologies Corporation, Japan) equipped with an energy-dispersive X-ray (EDX) spectrometer. X-ray photoelectron spectra (XPS) of the samples were also collected under vacuum (6.7×10^{-8} Pa) using ESCA5800 (ULVAC-PHI, Inc., Chigasaki, Japan) with Al Kα radiation (hv = 1486.6 eV). X-ray diffraction (XRD) analyses were also conducted by using X'Pert Pro by PANalytical, operated under a glancing beam configuration (0.5°) with Cu radiation.

Cyclic voltammetry (CV) and chronopotentiometry (CP) were conducted using a potentiostat and charge-discharge tester, respectively. A typical three-electrode electrochemical cell with a Pt black counter electrode, a saturated calomel electrode (SCE) reference electrode and the CNTs/Ni sample were used as the working electrode. The electrolyte was an aqueous KOH s solution (6 mol/L). CV was performed at 1, 10, 30, 50, 100 mV/s in a potential range of −0.05 to +0.35 V (in this article, potentials are documented vs SCE unless otherwise stated). CP was performed at 1 mA (5.6 A/g), 5

mA (27.8 A/g), 25 mA (138.9 A/g) in a potential range of −0.05 to +0.35 V. Before the capacitance measurements, the mass of the CNT/NiO$_x$(OH)$_y$ composite electrode was measured by electronic balance (Shimadzu AUW-220D). After the capacitance measurements, the composite layer (exposed to the electrolyte) were manually detached from SUS316 substrate and the mass of the electrode without the composite was measured. The difference between the mass values of the sample before and after the detaching was adopted as the real composite mass. EDX was used to know the elemental composition of the composite.

3. Results

3.1 SEM characterization

Figure 1a shows a surface view of CNTs film (after EPD and before Ni electrodeposition). CNTs with average diameter of 13 nm formed a nanoporous network. The thickness was approximately 1 μm, as estimated by optical microscopy. Figure 1b shows the CNT/Ni nanocomposite fabricated by pulsed electrodeposition at a low current density of 0.03 A/cm^2. Spherical nanoparticles with a diameter of 50 ± 20 nm were deposited on to the CNTs at a current density of 0.03 A/cm^2. Figure 1c shows the CNT/Ni nanocomposite fabricated by pulsed electrodeposition at a high maximum current density of 3 A/cm^2. Small (diameter of 7 ± 4 nm, calculated by the SEM image analyses) nanoparticles were deposited on to the CNTs at the high current density of 3 A/cm^2. EDX analyses showed the CNT/Ni contained approximately 35% by mass of Ni in the nanocomposites fabricated at both high and low current densities.

Previous studies of electrodeposited Ni nanoparticles on CNTs gave Ni particles with diameters larger than 15 nm [8,10,25,26]. In this study, Ni deposits with diameters less

than 10 nm were achieved, using pulsed electrodeposition applied at a maximum current density of 3 A/cm^2. This demonstrates that pulsed electrodeposition of Ni is effective for reducing the size of Ni deposits on CNT.

Figure 2 shows the SEM images of the CNT/NiO$_x$(OH)$_y$ nanocomposite fabricated by pulsed electrodeposition of Ni at 3 A/cm^2 and annealed in air at 523 K for 1 and 72 h. Comparison of Fig. 2a with that of the sample before annealing (Fig. 1c) revealed that the size and distribution of the deposits on the CNTs were unchanged by the 1-h annealing step. The Ni deposits maintained a fine dispersion during the annealing, suggesting a high surface area was also preserved. However, the 72-h annealed sample (Fig. 2b) showed a change of deposition texture, with deposits showing an average diameter of 15 nm. Sintering of Ni deposits is the likely cause of this change in the texture from 72-h annealing. On the other hand, XRD analyses on the samples showed no crystalline phases for Ni species, as shown in Fig. S2 in the Supplementary Data, suggesting that the Ni deposits are amorphous even after the annealing. Thus, unfortunately, the NiO/Ni(OH)$_2$ phase composition is unclear.

3.2 Electrochemical tests of capacitances

Figure 3 shows the CV curves of the CNT/NiO$_x$(OH)$_y$ nanocomposite fabricated by pulsed electrodeposition at 3 A/cm^2 and annealed in air at 523 K for 1 h. The CV curves featured clear redox peak pairs corresponding to the superficial Faradic reactions. The oxidation and reduction peaks were shifted to higher and lower potentials, respectively, with a midpoint potential of +0.16 V, as the scan rate increased. The symmetry of the CV curves suggested that the redox reactions were highly reversible, suggesting good potential for repeated cycling. The other samples fabricated under various conditions

also exhibited similar symmetric CV curves with redox peak pairs.

The specific capacitances (C) per mass of nanocomposite (approximately 0.5 mg) in each sample were determined from the CV curves using the following equation [14,19]:

$$C = \frac{1}{2m\Delta V} \int_{V_i}^{V_f} \frac{|I|}{(dV/dt)} dV , (1)$$

where m is the mass of nanocomposite, ΔV is the potential window, V_i and V_f are the starting and ending potentials in one cycle, respectively, I is the instantaneous current at a given potential and dV/dt is the scan rate.

Figure 4 summarizes the relationship between scan rate and specific capacitance per mass of CNT/NiO$_x$(OH)$_y$ nanocomposite, for samples fabricated under different conditions. Figure 4a shows specific capacitances of the CNT/Ni nanocomposite fabricated at a maximum current density of 3 and 0.03 mA/cm^2 and annealed in air at 523 K for 1 h. The specific capacitance of the CNT/Ni nanocomposite fabricated at 3 A/cm^2 was higher than that of the nanocomposite fabricated at 0.03 mA/cm^2. As observed in SEM images (Fig. 1c), Ni deposits on CNT were smaller (7 nm) in the nanocomposite fabricated at 3 A/cm^2. These particles therefore presented a larger surface area of active Ni than the sample fabricated at 0.03 A/cm^2. These results suggested the redox reactions and capacitive behavior were related to the nature of the Ni deposits.

The CNT/Ni nanocomposites fabricated at 3 A/cm^2 were annealed in air at various temperatures and durations. Figure 4b shows the effect of annealing conditions on the specific capacitances of CNT/NiO$_x$(OH)$_y$ nanocomposites (fabricated at 3 A/cm^2). High specific capacitances were obtained under the annealing conditions (T, t) = (523 K, 1 h), (523 K, 72 h) and (573 K, 72 h), where T is the annealing temperature and t is the annealing time. The annealing conditions (T, t) = (523 K, 1 h) gave nanocomposites

with the highest capacitance at low scan rates. The specific capacitance of the $(T, t) =$ (473 K, 72 h) sample was lower than other samples annealed at higher temperature and almost similar to that of the CNT/Ni sample without annealing. Figures 4c and 4d also indicate that the annealing conditions $(T, t) = (523$ K, 1 h) is the best.

The constant-current electrodeposition of Ni at 3 A/cm^2 for 0.5 s on CNTs has been conducted for comparison. Fig. S3 (in Supplementary Data) shows the SEM image of the sample fabricated by the constant-current electrodeposition of Ni and subsequent annealing at 523 K for 1 h. Ni-species particles with the average diameter of 40 nm were deposited on the CNTs. CV measurements revealed that the specific capacitance per mass of composites was 275, 172, 167, 112 F/g at the scan rates of 10, 30, 50 and 100 mV/s, respectively. The capacitance was much lower than that of the samples fabricated by the pulsed electrodeposition (Fig. 4). Thus, the advantage of the pulsed electrodeposition is the finer size of Ni deposits.

Figure 5 shows galvanostatic discharge curves from different discharge currents from the CNT/NiO$_x$(OH)$_y$ nanocomposite fabricated at 3 A/cm^2 and annealed in air at 523 K for 1 h. Higher discharge currents gave a shorter discharge time, consistent with previous results [13,14,16,18]. From the discharge curves, the specific capacitances (C) per mass of nanocomposite were derived using the following equation [18]:

$$C = \frac{I \Delta t}{m \Delta V} \text{, (2)}$$

where I is the discharge current, ΔV is the potential window, Δt is the discharge time in the potential window and m is mass of the nanocomposite. The specific capacitances per mass of nanocomposites were calculated to be 676, 490, 364 F/g at discharge currents of 5.6, 27.8, 138.9 A/g, respectively. The capacitance was higher at smaller discharge currents, in accordance with previous results [17,18,20,22]. The capacitances calculated

8

from the CP results were of the same order of those calculated from CV results.

We also performed 20000-cycle CP tests at 138.9 A/g of nanocomposite fabricated at maximum current density of 3 A/cm^2 and annealed in air at 523 K for 1 h. The results are shown in Fig. 6. The specific capacitance generally increased and stabilized after 10000 cycles, although the noticeable decrease and increase in the capacitance was observed at 8000 cycles (at this stage, the reason for the capacitance change at 8000 cycles are not understood). During subsequent cycles, the specific capacitance remained unchanged from the higher value. Charge/discharge curves (shown in the inset) revealed that the time for charge/discharge cycles became longer in the later cycles, owing to the increased capacitance (see Eq. (2)). This increase in capacitance could be explained by removal of contamination such as carbonaceous material and adsorbed gases on the CNT/Ni-species nanocomposites during the first 10000 charge/discharge cycles. These results demonstrated an excellent stability to repeated charge/discharge cycling of the CNT/Ni nanocomposites.

4. Discussion

As shown above, $(T, t) = (523$ K, 1 h$)$ was the best annealing condition. In this section, we focus on the effect of annealing time on the oxidation state and activity of Ni species, because annealing at 573 K may damage CNTs and alter the electric properties of not only Ni species but CNTs.

4.1 Surface states of deposited Ni

The Faradic reactions of Ni species are described by the following equations [31]:

$$NiO + OH^- \leftrightarrow NiOOH + e^- \quad (3)$$

$$Ni(OH)_2 + OH^- \leftrightarrow NiOOH + H_2O + e^- \quad (4).$$
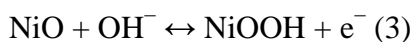
The equilibria between NiO and Ni(OH)$_2$ determines the electrochemical capacitance. Figure 7 gives the XPS of CNT/NiO$_x$(OH)$_y$ nanocomposites fabricated by pulsed electrodeposition at 3 A/cm^2 before and after annealing in air at 523 K. Before annealing, the surface of nanocomposite contained a large proportion of Ni(OH)$_2$ (856.0 eV [32,33] for Ni 2p$_{3/2}$ and 531.5 eV [34,35] for O 1s) as well as a smaller proportion of metallic Ni (852.8 eV [36]). This suggested that the majority of nanosized Ni deposits (Fig. 1c) were oxidized to form hydroxide during pulsed electrodeposition, water washing and drying in air. However, annealing at 523 K completely removed the metallic Ni component around 852.8 eV. Valence level XPS Spectra around 0 eV (Fig. 7c) also showed a decrease in intensity around 1.0 eV through annealing, which implied a decrease of metallic electronic states in the materials. Furthermore, the NiO component (854.4 eV [37–39] for Ni 2p$_{3/2}$ and 529.6 eV [40–42] for O 1s) increased with annealing time. The molar ratio of NiO/Ni(OH)$_2$ was calculated from XPS to be approximately 0.10 and 0.31 in the samples annealed for 1 and 72 h, respectively. The following dehydration reaction is suggested:

Ni(OH)$_2$ $\rightarrow$ NiO+H$_2$O (5).
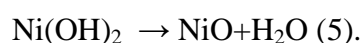
It is known that Ni(OH)$_2$ dehydrates at temperature greater than 523 K [23,34]. Thus, in the CNT/Ni nanocomposite annealed at $T < 473$ K, the only active Ni species is likely to be Ni(OH)$_2$, but when annealed at $T \geq 523$ K, some NiO states may become electrochemically active.

4.2 Specific capacitance per mass of active Ni species

The surface area of the active materials is an important factor affecting specific capacitance. We did not directly measure the surface area in this study, but performed a

relative comparison of the number and type (NiO and Ni(OH)$_2$) of active sites in the materials. The ratio of measured charge to the total theoretical charge of the active materials is the fraction of nickel sites, involved in the faradaic reaction, z, and can be estimated from the specific capacitance of the nanocomposite film by the following equation [19],

$$z = \frac{C_{Ni}\Delta V}{F/M}$$

where ΔV is the potential window, 0.4 V in this study, M is the average molecular weight of active Ni species, F is the Faraday constant, and C_{Ni} is the specific capacitance per mass of active Ni species (NiO and Ni(OH)$_2$) (F/g). C_{Ni} was calculated based on the compositional information from EDX spectroscopy and XPS.

Figure 8 shows the z value for the CNT/Ni nanocomposites fabricated at 3 A/cm^2 with and without annealing at 523 K. The z values of the sample with $(T, t) = (523$ K, 1 h) were markedly higher than those of other samples. This suggests an increase in the number of Faradic reaction sites following annealing in air at 523 K for 1 h. However, the z values of the sample with $(T, t) = (523$ K, 72 h) were low and similar to those of the sample without annealing.

Effect of surface oxidation states of Ni in Ni-based pseudocapacitors has been discussed in the previous studies [10,12,31]. Nam et al. [12] reported that NiO formation from Ni(OH)$_2$ by heating at 573 K is beneficial for stable pseudocapacitive behavior at high scan rates. However, they also reported that redox reaction of Ni(OH)$_2$ is responsible for the increased capacitance during repeated cyclic voltammetry. Wu and Hsieh [31] also showed that the surface area and electric conductivity of NiO was larger than that of Ni(OH)$_2$. Thus the NiO formation due to dehydration of Ni(OH)$_2$ during the annealing is likely to increase in specific capacitance, although the detailed mechanism

is still in debate. In this study, the sample with $(T, t) = (523 \text{ K}, 72 \text{ h})$ showed lower z values, despite featuring a higher NiO component at the surface compared with the sample with $(T, t) = (523 \text{ K}, 1 \text{ h})$ (Fig. 7). This was definitely attributed to the coarsened texture of active Ni deposits through prolonged (72 h) annealing (Fig. 2b). The reduced surface area of these Ni deposits resulted in deterioration of the specific capacitance. Thus, the finely dispersed structure of Ni nanoparticles with sub-10 nm diameters, rather than oxidation state of Ni, critically determines the high capacitance of Ni-based pseudocapacitors.

We performed additional CV measurements at a scan rate of 1 mV/s to compare the specific capacitance of these materials with other supercapacitors composed of Ni species. Figure 9 shows the specific capacitance per mass of active Ni species (NiO and $Ni(OH)_2$) (C_{Ni}, measured by CV) of the $CNT/NiO_x(OH)_y$ nanocomposite fabricated at 3 A/cm^2 and annealed in air at 523 K for 1 h, together with previous data from the literature [10,12,13–15]. C_{Ni} of capacitive electrodes generally decrease as the scan rate increases, as shown in Fig. 9. C_{Ni} of our CNT/Ni nanocomposites were higher than those of graphene oxide/NiO [13] and porous NiO [14] and comparable with those of other CNT/NiO_x composites [10,12,15]. This comparison suggests that CNT are effective for fast electron transfer in the CNT/Ni nanocomposite electrode.

Figure 10 shows C_{Ni} (measured by CP) of the CNT/Ni nanocomposite fabricated at 3 A/cm^2 and annealed in air at 523 K for 1 h. The maximum C_{Ni} was 1259 F/g at the a discharge current of 5.6 A/g, which is also comparable with C_{Ni} measured by CP in the previous studies [13,14,16,18,24].

4. Conclusions

In this study, CNT/NiO$_x$(OH)$_y$ nanocomposite films were synthesized by EPD of CNTs, the pulsed electrodeposition of Ni, followed by annealing steps. The materials were tested as electrochemical capacitors. Small (7 nm) Ni nanoparticles were uniformly deposited on the CNT surfaces by EPD. After annealing in air at 523 K for 1 h, specific capacitance per mass of active Ni species were measured as high as 1451 F/g at a scan rate of 1 mV/s. SEM images and XPS analyses of the samples revealed that NiO formation from dehydration of Ni(OH)$_2$ during annealing at 523 K was beneficial for the capacitance, but that long annealing times (72 h in this study) produced coarse, aggregated Ni deposits with decreased specific capacitance. In cyclic CP tests, the specific capacitance was maintained over 20,000 cycles at 138.9 A/g, which implied excellent durability. These results suggest that this porous structured CNT/NiO$_x$(OH)$_y$ nanocomposite is a promising material for supercapacitors.

Acknowledgments

References

[1] S. Iijima, Nature 354 (1991) 56–58.

[2] L. Hu, D. S. Hecht, G. Grüner, Chem. Rev. 110 (2010) 5790–5844.

[3] A. R. Boccaccini, J. Cho, J. A. Roether, B. J. C. Thomas, E. J. Minay, M. S. P.

Shaffer, Carbon 44 (2006) 3149–3160.

[4] S.-M. Bak, K.-H. Kim, C.-W. Lee, K.-B. Kim, J. Mater. Chem. 21 (2011) 1984–1990.

[5] K.-Y. Lin, W.-T. Tsai, J.-K. Chang, Int. J. Hydrogen Energy 35 (2010) 7555–7562.

[6] C.-Y. Chen, K.-Y. Lin, W.-T. Tsai, J-K. Chang, C.-M. Tseng, Int. J. Hydrogen Energy 35 (2010) 5490–5497.

[7] Z. Liu, Z. Li, F. Wang, J. Liu, J. Ji, K. C. Park, M. Endo, Mater. Res. Bull. 47 (2012) 338–343.

[8] C.-T. Hsieh, Y.-W. Chou, W.-Y. Chen, J. Solid State Electrochem. 12 (2008) 663–669.

[9] B. Gao, C.-Z. Yuan, L.-H. Su, L. Chen, X.-G. Zhang, J. Solid State Electrochem. 13 (2009) 1251–1257.

[10] B. Wen, S. Zhang, H. Fang, W. Liu, Z. Du, Mater. Chem. Phys. 131 (2011) 8–11.

[11] J. Y. Lee, K. Liang, K. H. An, Y. H. Lee, Synth. Metals 150 (2005) 153–157.

[12] K.-W. Nam, K.-H. Kim, E.-S. Lee, W.-S. Yoon, X.-Q. Yang, K.-B. Kim, J. Power Sources 182, (2008) 642–652.

[13] X. Zhu, H. Dai, J. Hu, L. Ding, L. Jiang J. Power Sources 203 (2012) 243–249.

[14] K. Liang, X. Tang, W. Hu, J. Mater. Chem. 22 (2012) 11062–11067.

[15] K.-W. Nam, E.-S. Lee, J.-H. Kim, Y.-H. Lee, K.-B. Kim, J. Electrochem. Soc. 152 (2005) A2123–A2129.

[16] C. Yuan, J. Li, L. Hou, L. Yang, L. Shen, X. Zhang, Electrochim. Acta 78 (2012) 532–538.

[17] Q. Lu, M. W. Lattanzi, Y. Chen, X. Kou, W. Li, X. Fan, K. M. Unruh, J. G. Chen, J. Q. Xiao, Angew. Chem. 123 (2011) 6979–6982

[18] M. Yang, J. X. Li, H. H. Li, L. W. Su, J. P. Wei, Z. Zhou, Phys. Chem. Chem. Phys. 14 (2012) 11048–11052.

[19] K.-W. Nam, K.-B. Kim, J. Electrochem. Soc. 149 (2002) A346–A354.

[20] A. G. Pandolfo, A. F. Hollenkamp, J. Power Sources 157 (2006) 11–27.

[21] Y.-G. Wang, X.-G. Zhang, Electrochim. Acta 49 (2004) 1957–1962.

[22] C.-C. Hu, M.-J. Liu, K.-H. Chang, J. Power Sources 163 (2007) 1126–1131.

[23] S. Chen, J. Zhu, X. Wu, Q. Han, X. Wang, ACS Nano 4 (2010) 2822–2830.

[24] D.-S. Kong, J.-M. Wang, H.-B. Shao, J.-Q. Zhang, C.-N. Cao, J. Alloy. Compd. 509 (2011) 5611–5616.

[25] Y. I. Golovin, D. Y. Golovin, A. V. Shuklinov, R. A. Stolyarov, V. M. Vasyukov, Tech. Phys. Lett. 37 (2011) 253–255.

[26] Z.-C. Wang, Z.-B. Qi, Q.-H. Liao, in: Proceedings of 2nd IEEE International Nanoelectronics Conference (INEC 2008), IEEE, 2008, pp. 539–541.

[27] N. Chopra, W. Shi, A. Bansal, Carbon 49 (2011) 3645–3662.

[28] N. Chopra, H. G. McWhinney, W. Shi, Mater. Charact. 62 (2011) 635–641.

[29] H. Natter, R. Hempelmann, Electrochim. Acta 49 (2003) 51–61.

[30] H. Natter, M. Schmelzer, R. Hempelmann, J. Mater. Res. 13 (1998) 1186–1197.

[31] M. S. Wu, H. H. Hsieh, Electrochim. Acta 53 (2008) 3427–3435.

[32] B. P. Löchel, H.-H. Strehblow, J. Electrochem. Soc. 131 (1984) 713–723.

[33] J. C. Klein, D. M. Hercules, J. Catal. 82 (1983) 424–441.

[34] P.-H. Lo, W.-T. Tsai, J.-T. Lee, M.-P. Hung, J. Electrochem. Soc. 142 (1995) 91–96.

[35] J. Haber, J. Stoch, L. Ungier, J. Electron Spectrosc. Relat. Phenom. 9 (1976) 459–467.

[36] A. N. Mansour, Surf. Sci. Spectra 3 (1994) 221–230.

[37] A. N. Mansour, Surf. Sci. Spectra 3 (1994) 231–238.

[38] K. Kishi, J. Electron Spectrosc. Relat. Phenom. 46 (1988) 237–247.

[39] R. B. Shalvoy, P. J. Reucroft, B. H. Davis, J. Catal. 56 (1979) 336–348.

[40] M. Oku, H. Tokuda, K. Hirokawa, J. Electron Spectrosc. Relat. Phenom. 53 (1991) 201–211.

[41] A. R. González-Elipe, R. Alvarez, J. P. Holgado, J. P. Espinos, G. Munuera, J. M. Sanz, Appl. Surf. Sci. 51 (1991) 19–26.

[42] P. H. Bolt, E. ten Grotenhuis, J. W. Geus, F. H. P. M. Habraken, Surf. Sci. 329 (1995) 227–240.

[43] W. Xing, F. Li, Z.-F. Yang, G. Q. Lu, J. Power Sources 134 (2004) 324–330.

Figure captions

Figure 1. SEM images of (a) electrophoretically deposited CNTs prior to pulsed electrodeposition of Ni, (b) CNT/Ni nanocomposite fabricated by pulsed electrodeposition of Ni at 0.03 A/cm^2, (c) CNT/Ni nanocomposite fabricated by pulsed electrodeposition of Ni at 3 A/cm^2.

Figure 2. SEM images of CNT/NiO$_x$(OH)$_y$ nanocomposite fabricated by pulsed electrodeposition of Ni at 3 A/cm^2 and annealed in air at 523 K for (a) 1 and (b) 72 h.

Figure 3. CV curves of CNT/NiO$_x$(OH)$_y$ nanocomposite fabricated by pulsed electrodeposition at 3 A/cm^2 and annealed in air at 523 K for 1 h. Scan rates of 10, 30, 50, 100 mV/s as indicated.

Figure 4. Relationship between specific capacitance per mass of CNT/NiO$_x$(OH)$_y$ nanocomposite and scan rate. Effects of (a) maximum current density during pulsed electrodeposition of Ni, (b) annealing conditions, (c) annealing temperature and (d)

annealing time are shown.

Figure 5. Galvanostatic discharge curves of the CNT/NiO$_x$(OH)$_y$ nanocomposite fabricated by pulsed electrodeposition at 3 A/cm^2 and annealed in air at 523 K for 1 h.

Figure 6. 20000-cycle charge-discharge test result of CNT/Ni nanocomposite fabricated at maximum current density of 3 A/cm^2 and annealed in air at 523 K for 1 h. Discharge current was set to 138.9 A/g. Galvanostatic charge/discharge curves of initial and final 4 s are shown in inset.

Figure 7. X-ray photoelectron spectra of CNT/Ni nanocomposites fabricated at 3 A/cm^2 with and without subsequent annealing for oxidation of Ni. (a) Ni 2p$_{3/2}$, (b) O 1 s and (c) valence band.

Figure 8. Fraction of Ni sites involved in Faradaic reaction of the CNT/Ni nanocomposite fabricated by pulsed electrodeposition of Ni at 3 A/cm^2 with and without annealing at 523 K as a function of scan rate in CV measurement.

Figure 9. Relationship between specific capacitances (measured by cyclic voltammetry) of Ni-species supercapacitors per mass of active Ni species and scan rate. The present results of CNT/NiO$_x$(OH)$_y$ nanocomposite fabricated at 3 A/cm^2 and annealed in air at 523 K for 1 h are also shown.
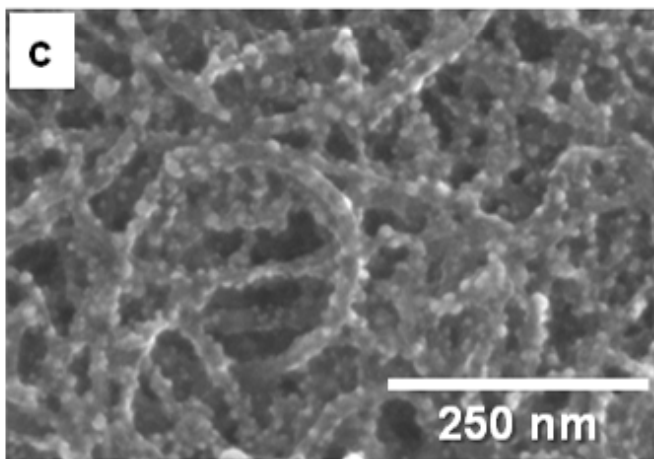
Figure 10. Relationship between specific capacitances (measured by chronopotentiometry) of Ni-species supercapacitors per mass of active Ni species and discharge current. The present results of CNT/NiO$_x$(OH)$_y$ nanocomposite fabricated at 3 A/cm^2 and annealed in air at 523 K for 1 h are also shown.
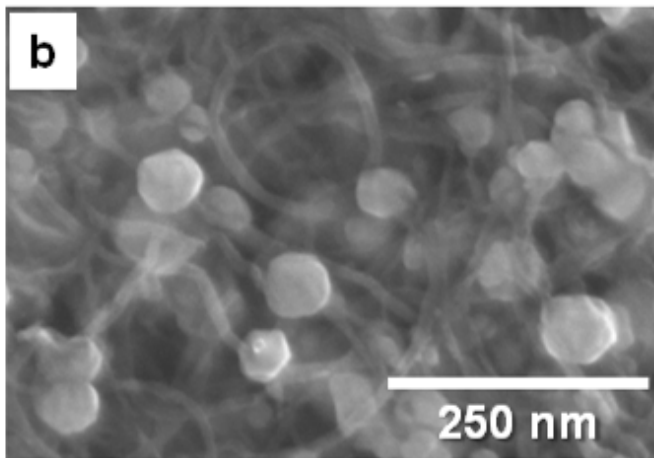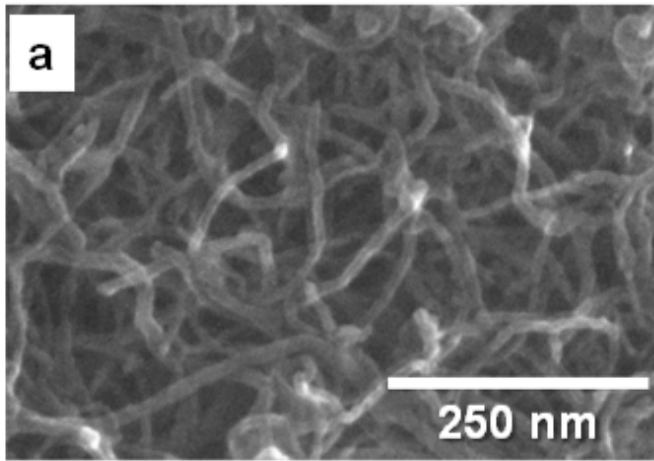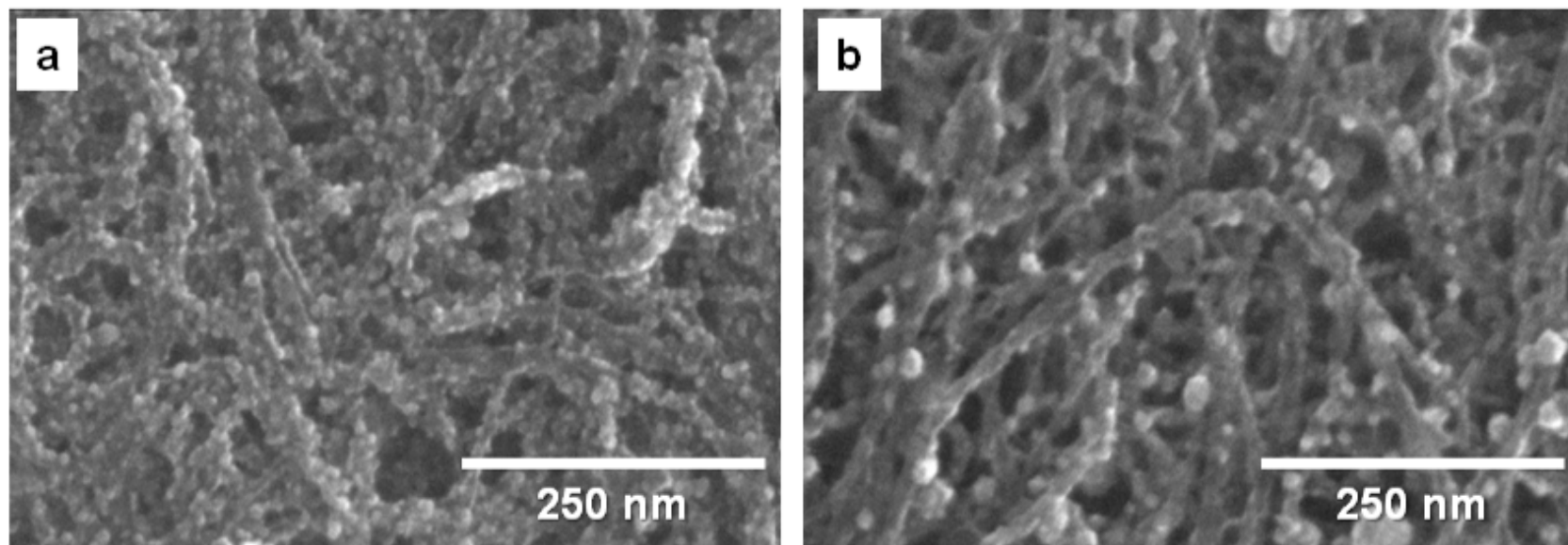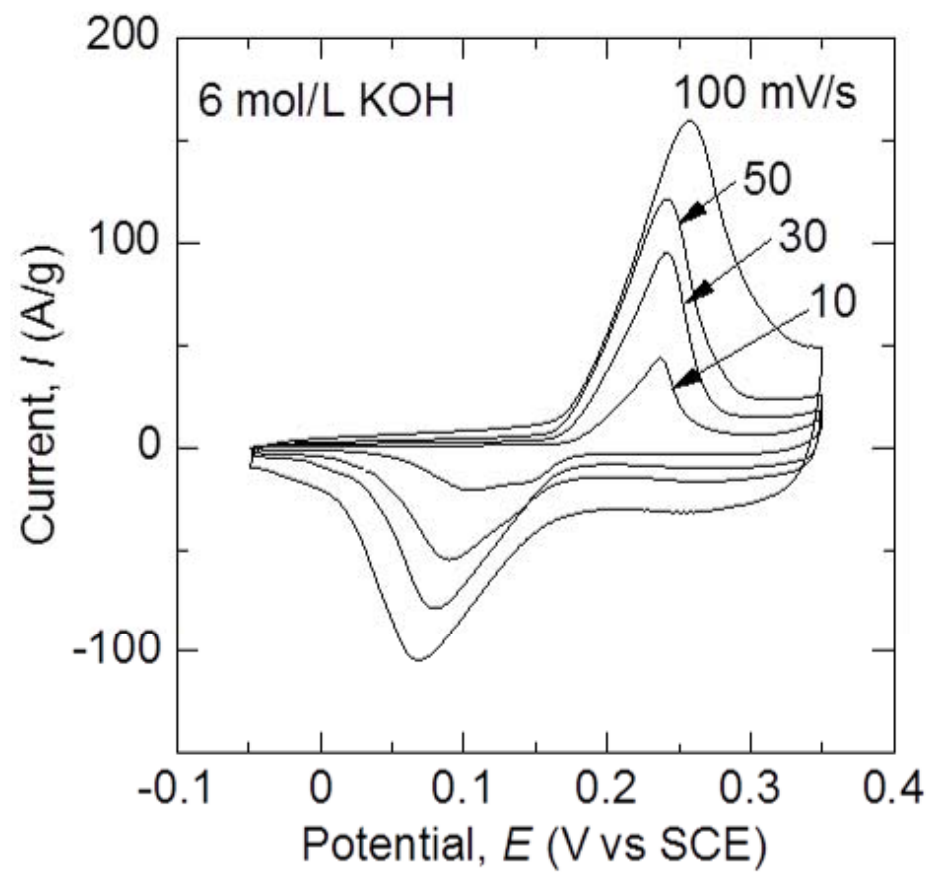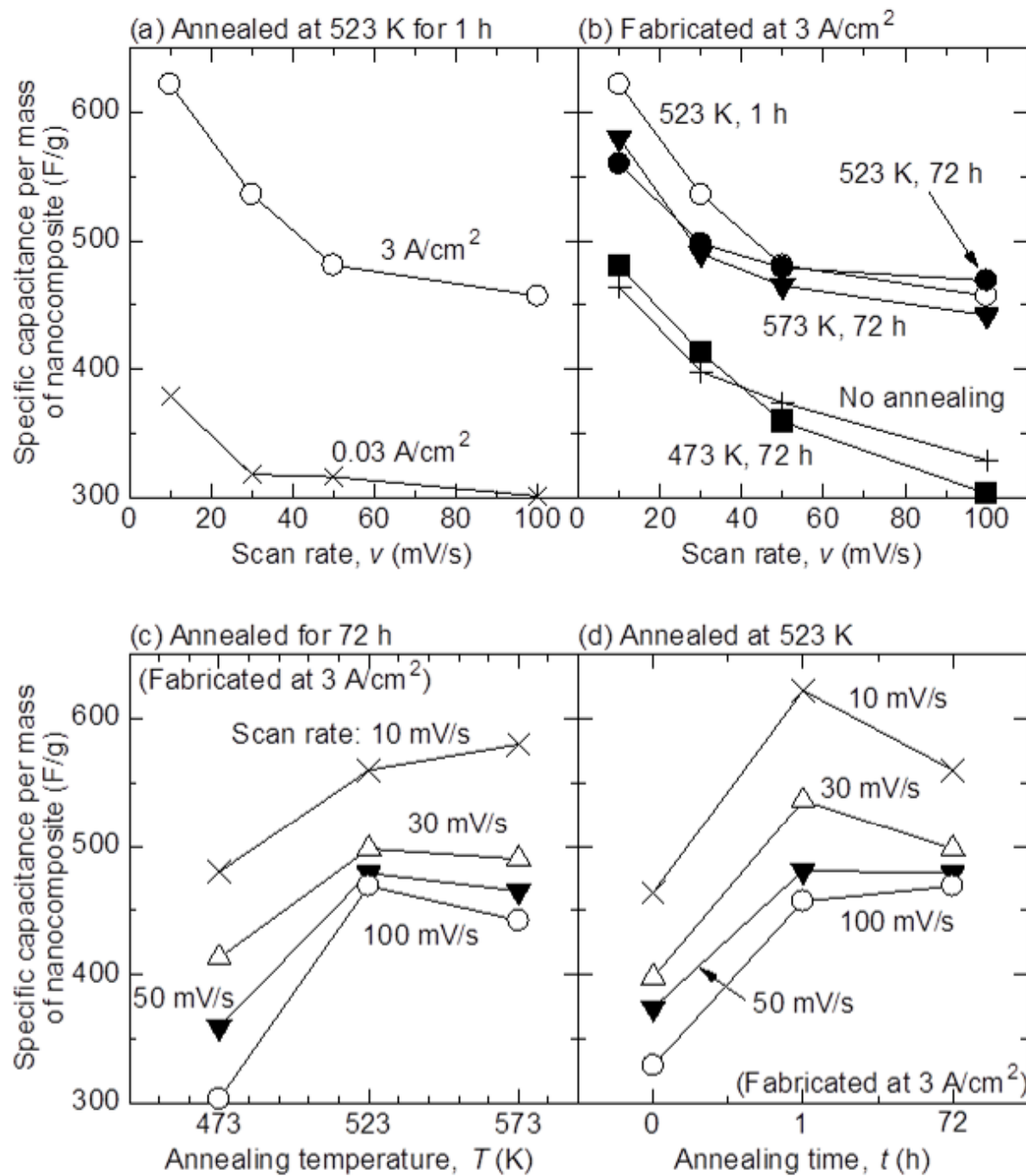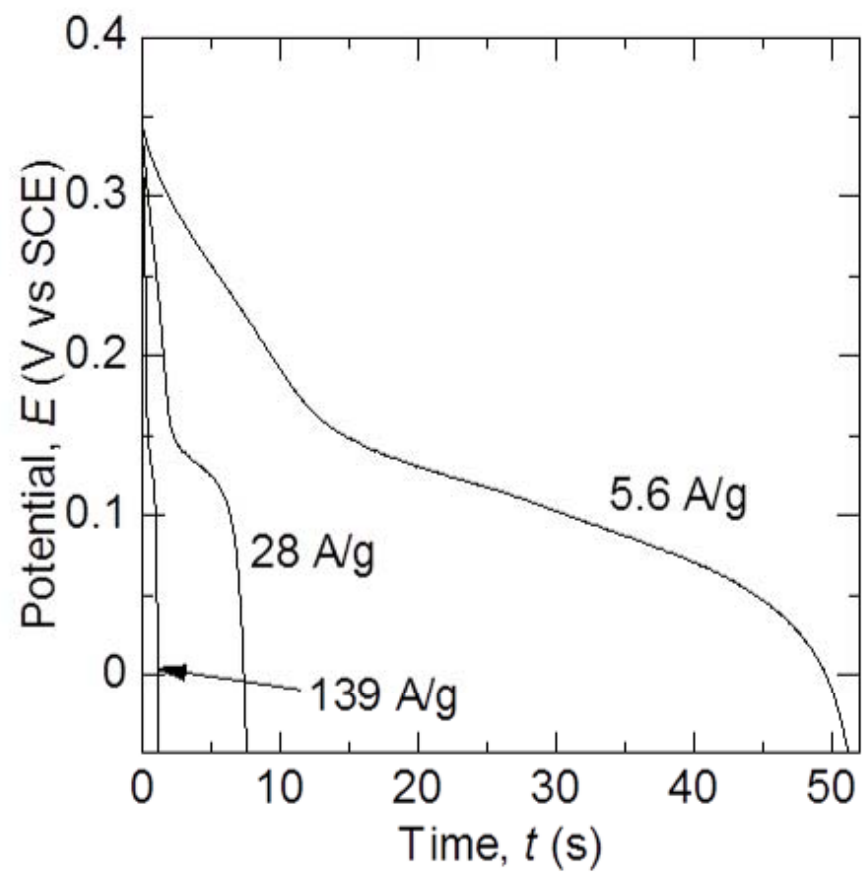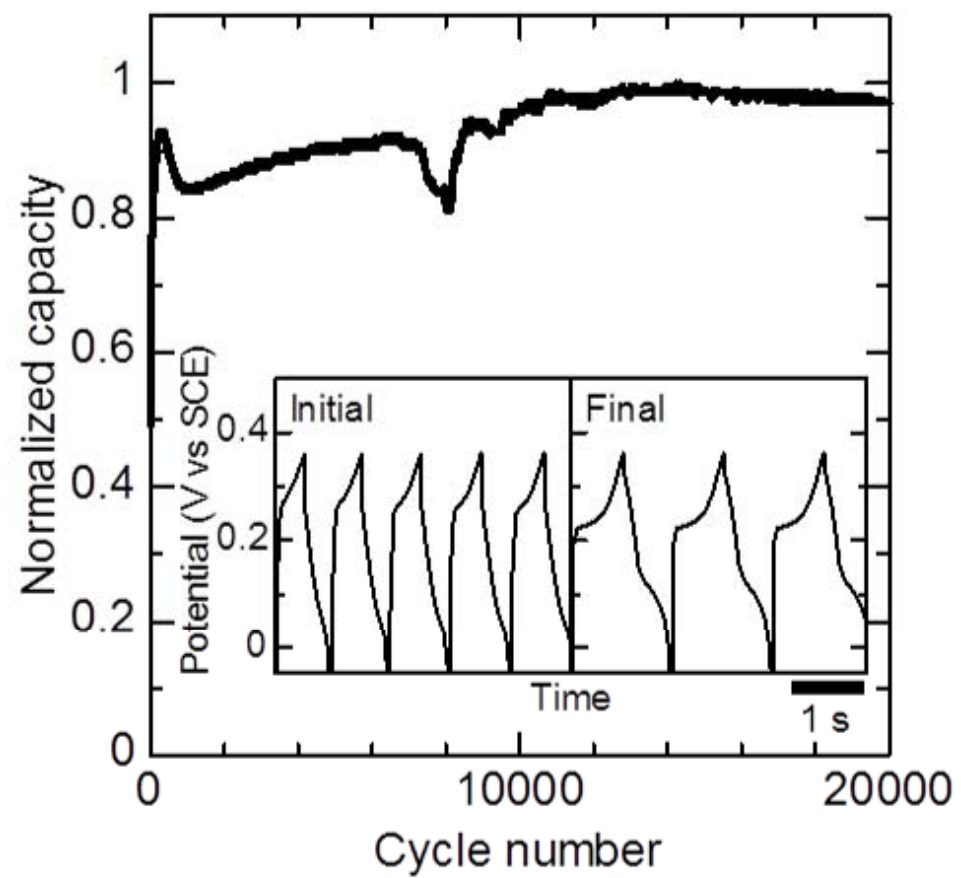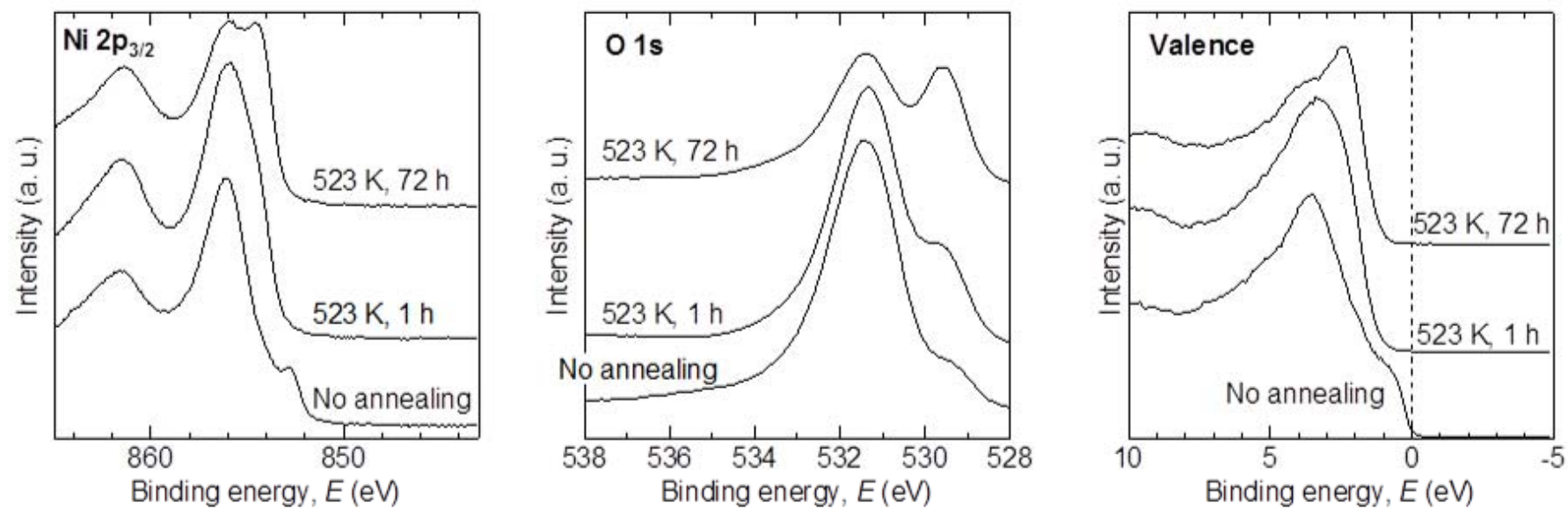
Figure 1.

Figure 2.

Figure 3.

Figure 4.

(a) Annealed at 523 K for 1 h

Specific capacitance per mass of nanocomposite (F/g)

3 A/cm^2

0.03 A/cm^2

Scan rate, v (mV/s)

(b) Fabricated at 3 A/cm^2

523 K, 1 h

523 K, 72 h

573 K, 72 h

No annealing

473 K, 72 h

Scan rate, v (mV/s)

(c) Annealed for 72 h
(Fabricated at 3 A/cm^2)

Specific capacitance per mass of nanocomposite (F/g)

Scan rate: 10 mV/s

30 mV/s

100 mV/s

50 mV/s

Annealing temperature, T (K)

(d) Annealed at 523 K

10 mV/s

30 mV/s

100 mV/s

50 mV/s

(Fabricated at 3 A/cm^2)

Annealing time, t (h)

Figure 5.

Figure 6.

Figure 7.

(Fabricated at 3 A/cm^2, annealed at 523 K)

Annealed for 1 h

72 h

No annealing

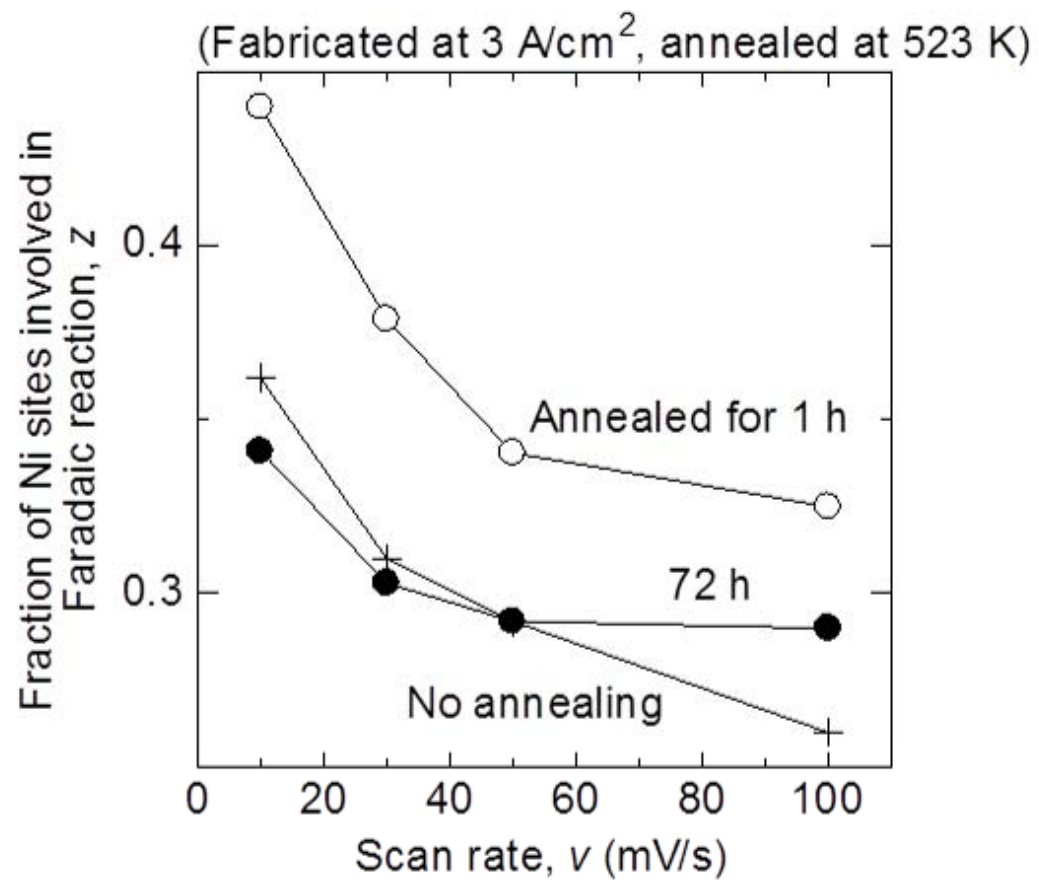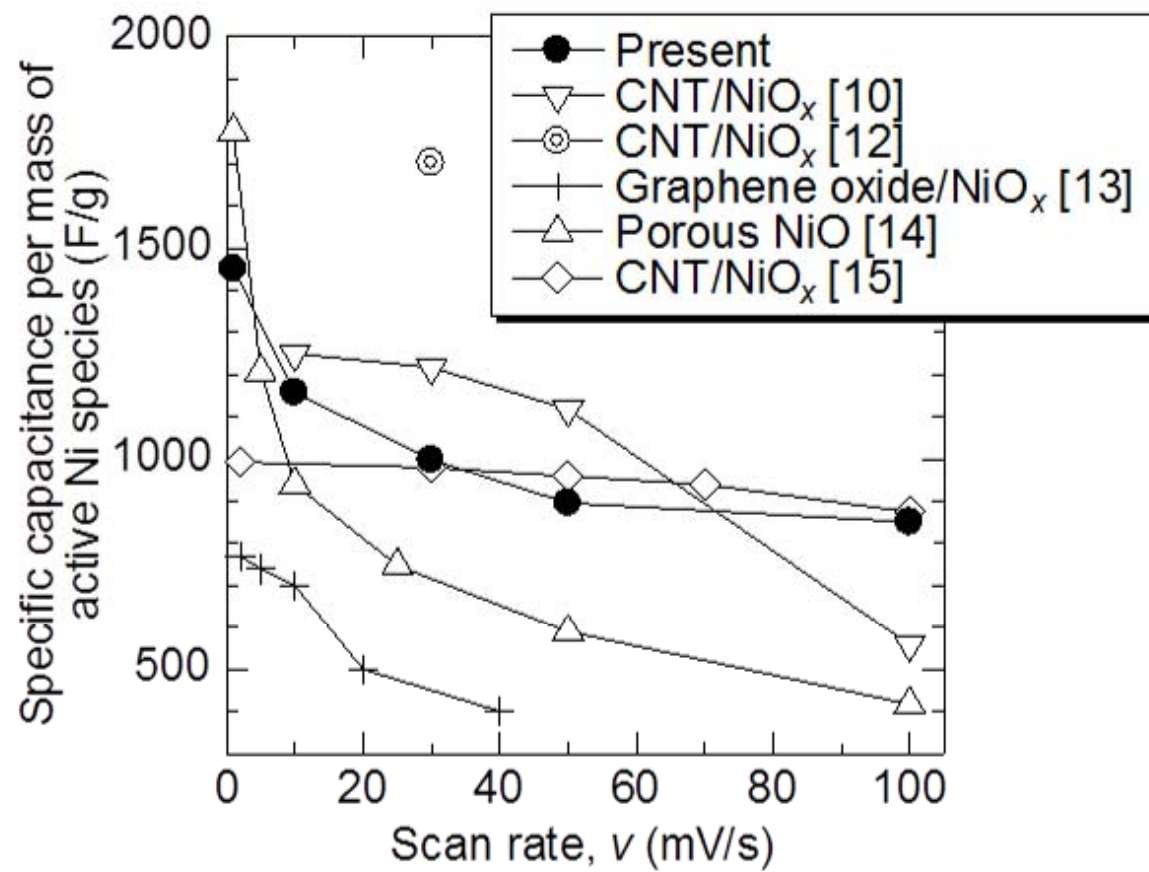Fraction of Ni sites involved in Faradaic reaction, z

Scan rate, v (mV/s)

Figure 8.

Figure 9.

Figure 10.